

WAVEGUIDES

CONTROLLING SOUND RADIATION

We have seen in past chapters that the radiation of sound from typical transducers is basically a fixed quantity. There appears to be little that we can do to affect the sound radiation response. The size and configuration determines the radiation pattern with the enclosure playing an important role at the lowest frequencies. If the driver is still radiating above the point where the enclosure is controlling the response then the response is pretty much completely dependent on the driver size. Little else has much of an effect.

In this chapter, we will study the concept of a waveguide as a directionality controlling device.

6.1 Historical Notes

It is important to go through the historical development of horn and waveguide theory in order to understand its evolution the current level of our understanding. The importance of this review stems from long-standing beliefs about waveguides and horns that are not in fact correct. Correcting these beliefs creates extreme limits on their applicability to current issues in their design.

Horns have been around for centuries and we have no idea when or where they were first used. Horns as musical instruments are certainly centuries old. With the advent of the phonograph, the horn was found to play a crucial role in amplifying the sound emitted from the small mechanical motions of the stylus. The horn was responsible for virtually all of the gain in the system. Its use therefore was principally one of a loading or impedance matching mechanism required to better match the high mechanical impedance of the stylus to the very low mechanical impedance of the medium – air. The horns role as an acoustic transformer is central to the evolution of horn theory.

When one is interested in the loading properties of a conduit, they need only be concerned with the average distribution of the acoustic variables across the diaphragm and hence across the conduit. This is, in fact, the assumption that Webster made when he derived what is now known as Webster's Horn Equation

$$\frac{1}{S(x)} \frac{\partial}{\partial x} S(x) \frac{\partial}{\partial x} \Psi(x) = \frac{1}{c^2} \frac{\partial^2 \Psi(x)}{\partial t^2} \quad (6.1.1)$$

It is commonly thought that this equation applies only to plane waves since Webster used a plane wave assumption in its derivation. However, this equation is far more broadly applicable than to plane waves alone. It is actually exact for any geometry where the scale factor of the coordinate of interest is one. The scale factor is a fundamental parameter of all coordinate systems as shown in Morse¹. (Having a scale factor is a requirement for separability.) The scale factors are known and can only be calculated for separable coordinate systems. The interesting thing to note is that any coordinate system which has a unity scale factor for any of its three dimensions is exact in Webster's formulation. Specifically these coordinates are:

- all three Cartesian Coordinates
- the axial coordinate in all Cylindrical Coordinate systems (Elliptic, Parabolic and Circular)
- the radial coordinate in the Cylindrical coordinate system
- the radial coordinate in Spherical Coordinates
- the radial coordinate in Conical Coordinates

The first two (six coordinates) apply to conduits of constant cross section, which are not very interesting to us. The useful ones are the three radial coordinates for the Cylindrical, Spherical, and Conical coordinate systems. It is extremely important to note two additional items. First, that there are only three useful coordinates in which Webster's equation is exact; and second, that all three of these have wave propagation in the other orthogonal coordinates. The importance of this last attribute will become clear later on.

If Webster's Equation is only correct in three useful situations then why is there so much literature surrounding its use? That is because the equation is still useful as an approximation to any conduit of varying cross section. In nearly all of the common cases of the application of Webster's equation it is used as an approximation to the actual wave propagation in a flared conduit. There has also been a great deal of literature written about the application of Webster's equation to the evaluation of these approximate solutions. Almost nothing has been written about when these approximations are "good" approximations and when we should be suspect of their validity.

The only place where we have seen such a discussion is, once again, in Morse² where they state:

Both pressure and fluid velocity obey this modified Wave Equation, which approximately takes into account the variation of cross sectional size with x . The equation is a good approximation as long as the magnitude of the rate of change of \sqrt{S} with x is much smaller than unity (as long as the tube "flares" slowly).

1. See Morse, *Methods of Theoretical Physics*

2. See Morse, *Methods of Theoretical Physics*, pg. 1352

These are very limiting conditions that have been almost universally ignored. Let us look at what they imply about the development of the well know exponential horn.

Restating Morse, as applied to an exponential horn, let

$$S(x) = S_0 e^{mx} \tag{6.1.2}$$

we can see that, for this example, Webster’s equation is “good” only so long as

$$\left| \frac{d}{dx} \sqrt{S_0 e^{mx}} \right| \ll 1.0 \tag{6.1.3}$$

$S_0 =$ the throat area

$m =$ the flare rate

The horn contour for this example is shown in Fig.6-1. This figure shows an

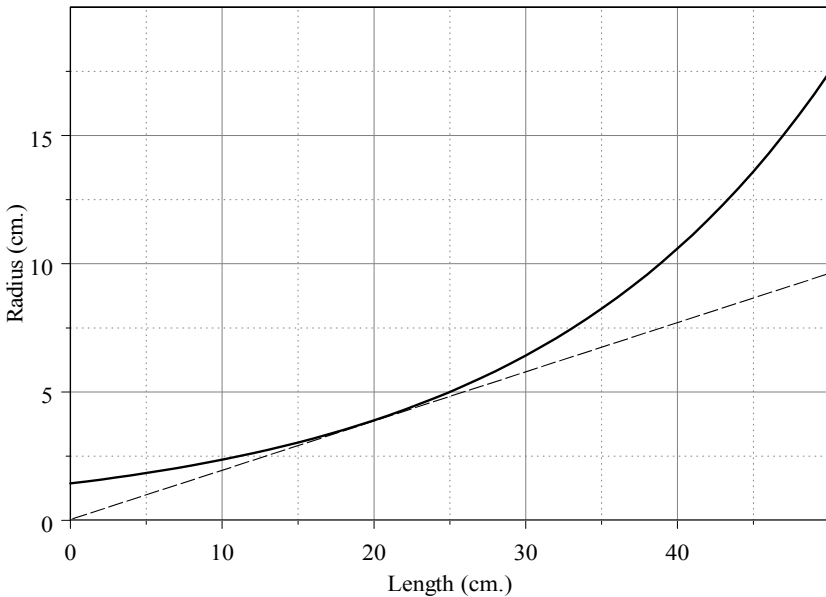


Figure 6-1 - A typical exponential horn contour

exponential horn contour of typical shape and length. In Fig.6-1, we have plotted the value of Eq.(6.1.3) as a function of the axial distance from the throat. These figures show that the assumptions for an accurate application of Webster’s Equation to an exponential horn are clearly violated for a length of the horn beyond about 15-20cm (Morse says much less than 1.0, but how much less is a matter of choice. We ascribe here to the use of a value of .5 as being the limit of accuracy, the assumptions being completely invalid at the value of 1.0.)

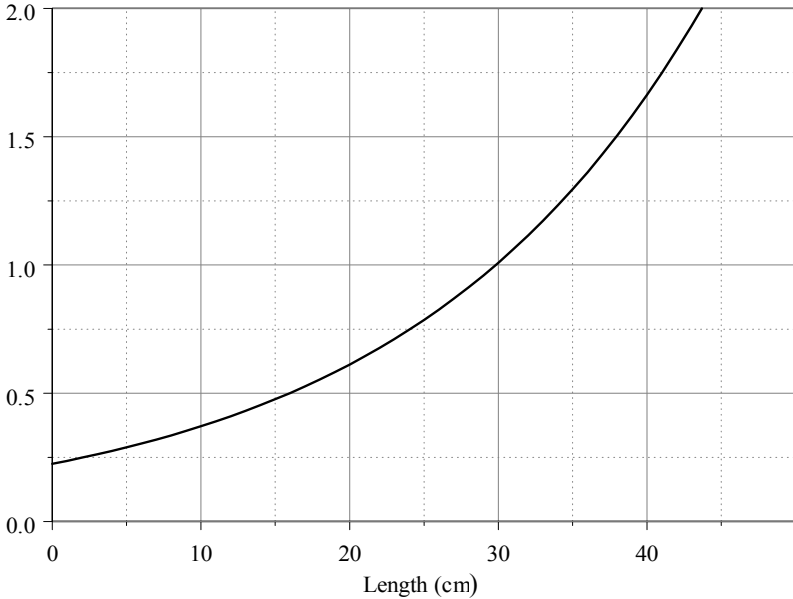


Figure 6-1 - Plot of Eq.(6.1.3)

In Fig 6-1, we have shown a line drawn tangent to the horn contour and originating at the center of the throat, the acoustic center of the throat's wavefront. A simple rule of thumb that we use is that any contour which lies past this point of tangency cannot be accurately described by Webster's equation. This rule of thumb implies a geometrical interpretation of the limitation of Webster's equation. The horn equation cannot predict the wavefronts once they are required to diffract around a point along the device that places the receding boundary in the shadow zone of the acoustic center of the originating wavefronts. Fig.6-1 shows that the only exponential horn which could be accurately represented by the Webster equation is extremely short. A horn of this length is of no practical interest.

Further support for our "rule of thumb" comes from considering Huygens' principle and the construction of Huygen wavefronts. Beyond the point of tangency, wavefronts, if they are to remain perpendicular to the sides of the conduit (as they must), have to have an apparent acoustic center which is front of the actual throat of the device. Huygen's principle allows for un-diffracted wavefronts to be flatter than those from the acoustic center, but it does not allow for a wavefront curvature to be less than the radius to the acoustic center. A little thought will show why this must be true. So stated another way, our rule of thumb becomes: horn wavefronts with a curvature less than the radius to the throat must have diffracted somewhere along the trip down the device - the diffraction creating a new acoustic center from which wavefronts emerge.

It is further interesting to note that in those cases where Webster's Equation is exact, there is never a point on the contour of the horn which is in the shadow

zone, i.e. our “rule of thumb” is never violated. The overwhelming majority of work done in horn theory suffers from a serious question of its validity.

How one gets around this problem leads us into another line of reasoning for which there are two paths. We could join the exponential section of the above contour to a spherical section continuing out from the point of tangency to the acoustic center line, thus insuring that our rule of thumb was never violated. This does in fact work reasonably well, and is in common usage. However, the fact remains that the exponential section is still only an approximation and we really don't know the actual shape of the wavefront at the joining point. As we shall see later, this is a serious limitation to the joining approach.

Now that we have shown that the horn equation has severe limitations in its applicability to important problems in waveguides, we will discuss how these limitations might affect the expected results of using it. As we showed in Chap.3, if we know the wave shape of the wavefront as it crosses through a boundary for which we have a radiation solution (flat, spherical or cylindrical), then we can achieve a fairly accurate prediction of the directivity of this source. However, we must know the *précis* magnitude and phase of the wavefront at every point in the aperture in order to do this calculation. From the above discussion, we should have serious doubts about the ability of Eq.(6.1.1) to give us this information, except, of course in those limited cases where it is exact. The natural question to ask is: can we develop an equation or an approach which will allow us to know, with some certainty, what the magnitude and phase is at every point within the waveguide? The answer is yes, but the price that we must pay for this precious knowledge is a substantial increase in the complexity of the equations and their solution.

6.2 Waveguide Theory³

As we discussed above, the early use of a horn was substantially different than what we are attempting to develop here. The early need for horns was as an acoustic loading devices and our interest here is in controlling source directivity. (Loading essentially became a non-issue with the almost unlimited amplifier power capability available today.) For this reason, we will adapt the terminology that a horn is a device which was developed with Webster's Equation and its approach to calculation (wherein, only the average wavefront shape and the acoustic loading is required) and a waveguide is a device whose principal use is to control the directivity. A waveguides design is along the lines that we will develop in the following sections, a horns design using Webster's equation. The acoustic loading of a waveguide can usually be calculated without much trouble, but not always. However, since loading is not a central concern for us this limitation is not significant.

3. See Geddes “Waveguide Theory” and “Waveguide Theory Revisited”, *JAES*.

We know from earlier chapters that the Wave Equation is always accurate so long as we can apply the proper boundary conditions. This can happen only in one of a limited set of coordinate systems. Take, as an example, the simple case of a conduit in a spherical geometry as shown in Fig.6-2. The boundary conditions

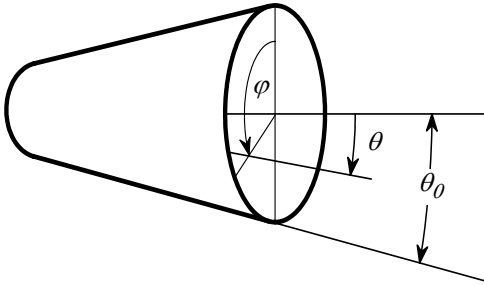


Figure 6-2 - A simple horn-waveguide example

here are that the conduit is symmetric in φ , and has a θ velocity which is zero at some θ_0 . For now we will not worry about the terminations of this conduit along its axis and simply assume that it is semi-infinite. In other words it has a finite throat, but a mouth at infinity.

We can use either the full Wave Equation, or Eq.(6.1.1) in this example because of its simplicity. We have already discussed the horn approach so let's use the full Wave Equation as we developed in Chap.3. We know that the following solution applies in both the Spherical coordinate system and Webster's Equation.

$$\Psi(r) = A \frac{e^{ikr}}{r} + B \frac{e^{-ikr}}{r} \quad (6.2.4)$$

We can immediately see from this solution that there is one aspect to the Wave Equation approach that is not present in Webster's approach. That is, we know from the Wave Equation that the wave number k is a coupling constant to two other equations in θ and φ . We can exclude the coupling to φ since there is no φ variation in the boundary conditions, but we cannot simply make the assumption that there is no variation of the waves in θ . If there is a θ dependence of the wavefront at the throat (or any point for that matter) then there will be a θ dependence in the wave as it is propagates down the device. This is significantly different from Webster's approach since Webster's equation does not allow for any θ dependence. This limitation is actually far more significant than the errors due to the flare rate that we discussed above.

As an example, consider evaluating a "conical" horn versus a Spherical waveguide (both are as shown in Fig.6-2) using Webster's equation and the acoustic waveguide approaches respectively. Horn theory yields an impedance at the throat, but it yields no information about the amplitude and phase of the wavefront anywhere within the device. The assumption of uniform amplitude across

the device means that Webster’s approach predicts the same value at every point on some (unknown) surface which is orthogonal to the horn boundaries. Of course we could argue (correct in some cases) that the wavefront must be a spherical section at every point. But what happens if the device is fed at the throat with a plane wave? There is simply no way to answer this question with the tools available to us from Webster.

Consider now the alternate waveguide approach. From Sec. 3.4 on page 49 we know that the solutions for the radial coordinate are

$$\Psi(r) = A h_m^{(1)}(k_r r) + B h_m^{(2)}(k_r r) \tag{6.2.5}$$

If the driving wavefront is of a spherical shape, then only a single mode $m = 0$ will be excited. In that case we get the same answer for a wave propagating down the device for either the Horn Equation or the Wave Equation

$$\begin{aligned} \Psi(r) &= A h_0^{(1)}(kr) + B h_0^{(2)}(kr) \\ &= A \frac{e^{ikr}}{r} + B \frac{e^{-ikr}}{r} \end{aligned} \tag{6.2.6}$$

where $k_r = k$, since it is always in the r direction in this case. However, we also know that there are an infinite number of other possibilities where $m \neq 0$. Only the Wave Equation approach offers up this added flexibility in its application.

When the throat is driven by a wavefront which does not coincide with a spherical section of the same radius as the throat, then the wavefront can be expanded into a series of admissible wavefronts prior to propagation down the device. Since we have solutions for all of these waves, we can develop the final solution as a sum over these various wave orders.

Consider a plane wave excitation at the throat. It is well known that a plane wave can be expanded into an infinite series of spherical waves. This series is

$$p(\text{plane wave}) = A \sum_{m=0}^{\infty} (2m+1) i^m j_m(ka_0) P_m(\cos\theta) \tag{6.2.7}$$

$a_0 = \text{the radius to the throat}^4$

Basically, the Legendre Polynomials form an expansion with the weighting factors given by the terms to the left of them. Eq.(6.2.7) is applicable to a plane pressure wave – a scalar function. If we had a planar velocity source at the throat (i.e., a flat piston) then we would have to match this to the radial and angular velocities at the throat. This would not actually be too difficult, except that there is yet another problem with this approach, so we will leave this discussion for later in order to address the solution to our current problem.

Unfortunately, the Legendre Polynomials, as shown in Eq.(6.2.7), do not fit the boundary conditions of our waveguide, that is, they do not have a zero slope

4. See Morse, *Any text*

at the walls of the waveguide, $\theta = \theta_0$ for all m . The normal Legendre Polynomials must have a separation constant m which is an integer because of periodicity. The new functions can no longer require this constant to be an integer. (Why?) Compare the two plots in Fig.6-3. The right side of the plot shows the normal Legendre Polynomials over a 30° arc. The left side shows the Modified Legendre Polynomials (modified because of the new separation constant ν_m) that meet the boundary conditions at the walls of the waveguide. The new polynomials can be used to expand any axi-symmetric source at the throat – they form a complete orthogonal set. It is worth noting the similarity of Fig.6-3 with Fig.4-3 on page 73.

Thus far we have seen that by utilizing the full machinery of the Wave Equation we can match any velocity distribution placed at the throat of a waveguide so long as this waveguide lies along a coordinate surface of one of the separable coordinate systems (although we have as yet only looked at a very simple one). We have also seen that this wavefront matching cannot be accomplished by using Webster’s horn equation; the machinery to do so just does not exist in that formulation. Of course we could force the throat wavefront to match the lowest order mode of the horn and then the horn equation would be accurate, exact in fact.

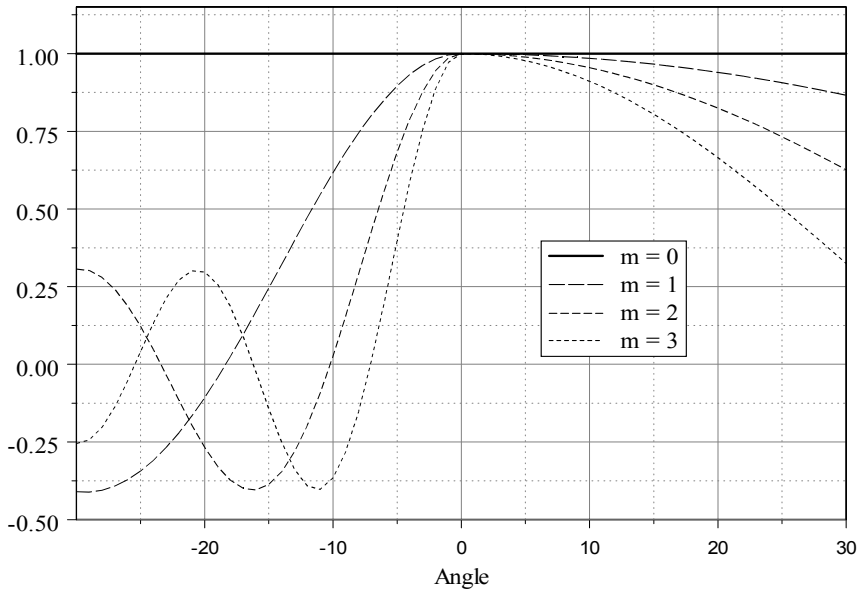


Figure 6-3 - Normal Legendre Polynomials (right) for 30° waveguide (left)

The problem is that there are no sources which have a velocity profile that matches any of the three geometries which have an exact horn solution!

In order to continue we have a choice of three alternatives:

- accurately use the horn equation with unrealistic sources
- use approximate solutions for real sources, or
- obtain exact solutions for realistic sources but restricting ourselves to the use of a few prescribed geometries (separable coordinate systems) for which an exact analysis is possible

The first choice is not of interest to us. The second choice may be workable and we will investigate that alternative later, but for now we will choose the third option in order to get exact answers, which we can use later as a comparison to the approximate solutions. We will also get a better understanding of the nature of the exact solution.

Returning to the above example, we can see that a planar source at the throat of a Spherical waveguide will have more than a single mode of propagation due to the required fitting of this source to the waveguide at the throat. By expanding the source velocity in a series of modified Legendre Polynomials, we can determine the contribution of the various modes of the waveguide. We saw an example of this in Sec.4.5 on page 83 where we expanded a spherical wavefront in terms of a set of plane aperture modes. We are now doing the reverse, namely, expanding a plane wave in an aperture in terms of a set of finite angular spherical modes. The two processes are completely analogous albeit reversed.

Each of the waveguide modes will propagate with a different phase and amplitude which can readily be calculated as

$$p(r, \theta) = \sum_m A_m(k) P_{v_m}(\cos \theta) h_{v_m}^{(2)}(kr) \quad (6.2.8)$$

v_m = the m th Eigenvalue for the waveguide

The eigenvalues v_m need to be determined specifically for each waveguide since they vary with the angle of the walls. The function $h_{v_m}^{(2)}(kr)$ is the same Spherical Hankel Function (of the second kind – outgoing) that we have seen before except that now these functions have a non-integer order. The calculation of these functions is not difficult although the details are beyond the scope of this text and covered elsewhere⁵.

As we saw in Sec.4.2, the modes radiate (propagate in the current case) with efficiencies which vary with frequency. Fig.6-4 shows the modal impedances for the first three modes in a 30° Spherical waveguide. From this figure, we can see precisely the differences in horn theory and waveguide theory.

Horn theory yields only the solid line shown in this figure, which is exactly the same as the waveguide calculation for this lowest order mode. Above $ka \approx 2\pi$ (where a is the radius of the waveguide's throat), the first mode begins to cut-in.

5. See Zhang, *Computation of Special Functions*

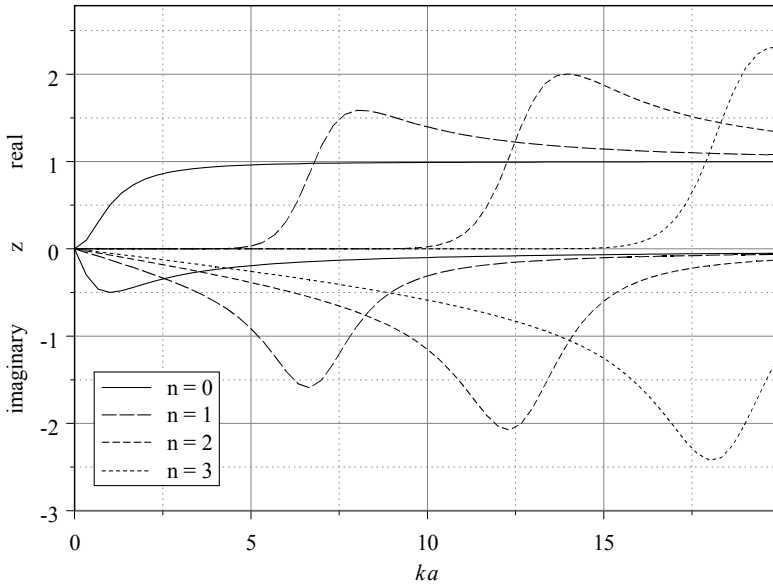


Figure 6-4 - Real and imaginary parts of the modal impedances for a 30°

Below this frequency both the horn theory of Webster and waveguide theory will yield nearly identical results (a small difference is due to the finite imaginary part of the higher order modes). Above this frequency the first mode (which would be quite significant for a piston source driving a Spherical waveguide) has an even greater proportional effect on the wavefront than the zero order mode, and could hardly be ignored for accurate results. It is in this region (above cut-in of the first mode) that horn theory has serious shortcomings. Its validity becomes progressively worse as the frequency goes up and even more modes cut-in. Waveguide theory remains accurate to as high a value as one cares to calculate its modes. This is a significant difference in accuracy for a large directivity controlling device.

Now that we have seen why waveguide theory is preferable to horn theory for high frequency directivity controlling devices, we will investigate the various separable coordinate systems for which waveguide theory is directly applicable in order to determine which ones have useful geometries.

6.3 Waveguide Geometries

We have already discussed several of the separable coordinate systems, but below is a table of the complete set of 11 along with the type of source that is required at the throat for a pure zero order mode.

Name	Coordinate	Source Aperture	Source Curvature	Mouth Curvature
Rectangular	any	rectangle	flat	flat
Circular Cylinder	radial	rectangle	cylindrical	cylindrical
Elliptic Cylinder	radial	rectangle	Flat	cylindrical
Parabolic Cylinder	none			
Spherical	radial	circular	spherical	spherical
Conical	radial	elliptical	spherical	spherical
Parabolic	none			
Prolate Spheroidal	radial	rectangle	cylindrical	spherical
Oblate Spheroidal	radial	circular	flat	spherical
Ellipsoidal	radial	elliptical	flat	spherical
Paraboloidal	none			

Table 6.1: Useful waveguides for Separable Coordinates

All of the useful coordinates are radial and all of the mouth apertures are the same as the throat apertures (not shown). The source apertures are either rectangular or elliptical (circular being a special case of elliptical). The mouth curvatures (radiation wavefronts) can only be spherical or cylindrical, flat being of little interest. This last feature is the main reason why we studied the geometries that we did in Chap. 4. If the apertures are circular then the physical device must be axi-symmetric. The wave propagation need not be axi-symmetric, however. We will not look into this possibility since it is rather unusual in practice.

It is also possible to combine waveguides to create new devices. For example, the Prolate Spheroidal (PS) waveguide takes a square cylindrically curved wavefront at its throat, which is exactly what an Elliptic Cylinder waveguide produces. A waveguide created as a combination of two waveguides in these two coordinate systems would take a square flat wavefront as input and produce a square spherical one.

It is interesting to note that the horn equation is only exact when the input and output wavefront curvatures remain unchanged. By this we mean that the location of the center of radius of the wavefront for both the throat and the

mouth does not move in space. This is exactly what it means to have a unity scale factor. Unfortunately, geometries that do not have unity scale factors are significantly more difficult to analyze – the price that we must pay for the higher accuracy of the waveguide approach. We have already looked at a Spherical waveguide in some detail and now we will investigate a waveguide that is based on the Oblate Spheroidal (OS) coordinate system in order to compare and contrast its characteristics with those that we have already studied.

6.4 The Oblate Spheroidal Waveguide

Proceeding as in the previous sections, the first calculations that we need to do for an OS waveguide are to determine the wave functions (or Eigenfunctions) in this coordinate system. Unlike the previous case of the Spherical Wave Equation, the wave functions for the OS coordinate system are not as readily available. The unique thing about those coordinate systems that do not have unity scale factors is; even though the equations separate in the spatial coordinates they remain coupled through the separation constants (the wavenumber or time coordinate). We have not encountered this complication in any of the problems that we have studied thus far. The wave functions in both the radial coordinate and the angular coordinate will be found to depend on a common parameter $\mathbf{c}=kd$, where d is the inter-focal separation distance (See Fig 1-2 on pg.6). (We must be careful not to confuse this \mathbf{c} (non-italic-bold) with the wave velocity c , of the same letter. The use of \mathbf{c} is historical and the authors do not feel privileged enough to change it.)

The separated Wave Equation in OS Coordinates is

$$\frac{d}{d\eta} \left[(1-\eta^2) \frac{d S_n(\mathbf{c},\eta)}{d\eta} \right] + \left[\lambda_n(\mathbf{c}) + \mathbf{c}^2 \eta^2 \right] S_n(\mathbf{c},\eta) = 0 \tag{6.4.9}$$

and

$$\frac{d}{d\xi} \left[(\xi^2 - 1) \frac{d R_n(\mathbf{c},\xi)}{d\xi} \right] - \left[\lambda_n(\mathbf{c}) + \mathbf{c}^2 \eta^2 \right] R_n(\mathbf{c},\xi) = 0 \tag{6.4.10}$$

$S_n(\mathbf{c},\eta)$ = *The angular wave functions of order n (axi-symmetry assumed)*

$R_n(\mathbf{c},\xi)$ = *the radial wave functions of order n*

$\lambda_n(\mathbf{c})$ = *the Eigenvalue for wave functions*

For brevity, we have already simplified these equations by assuming axi-symmetric wave propagation around the waveguide and set the value of $m=0$ (m is the traditional constant for the φ coordinate and found in most texts on OS and PS wave functions). All of the published information on the OS wave functions assumes periodicity in η , which is a different boundary condition than what we require here. We must apply a zero η velocity (zero gradient) boundary condition at the walls just as we did in the previous section. Unfortunately, none of the published tables and subroutines which are readily available can be applied to our problem.

We will need to revise the techniques used in the published literature and apply them to the specific boundary conditions for our particular problem. To do this, we will use a differential equation solution technique known as “shooting.”⁶

We must first calculate the Eigenvalues $\lambda_n(\mathbf{c})$ for the boundary conditions of our problem. These boundary conditions are

$$\left. \frac{d S_n(\mathbf{c}, \eta)}{d \eta} \right|_{\eta=\cos \theta_0} = 0 \tag{6.4.11}$$

and

$$S_n(\mathbf{c}, \eta) \Big|_{\eta=1} = 1.0 \tag{6.4.12}$$

The first condition allows us to only consider functions which are symmetric about $\eta=1$. This means that only even values of ν will be considered. By starting at $\eta=1$ and $\mathbf{c}=0$ we “shoot” to the point $\eta=\cos \theta_0$, where θ_0 is the design angle of the waveguide, and enforce a boundary condition on the slope of these functions to be zero at that point. A point of clarification here: the design angle is not necessarily the “coverage” angle of the device. This issue will be investigated in more detail later on, but for now, it is important to note that here θ_0 refers to the physical angle of the walls of the waveguide.

The Eigenvalues are known for $\mathbf{c}=0$, from the spherical case, and they are $\lambda_n(0)=n(n+1)$. It is also known that the Eigenvalues will decrease as \mathbf{c} increases at a constant rate. Using these approximations to the Eigenvalues as starting values, we calculate the exact Eigenvalues for any given value of \mathbf{c} by “shooting” from one boundary to the other. The Eigenvalue is adjusted until a satisfactory match has been achieved between the boundary conditions at the two end points. Once we have the Eigenvalue we simply use standard numerical integration to compile the angular functions $S_n(\mathbf{c}, \eta)$ (where $\eta=\cos \theta$).

Using the Eigenvalues calculated from the above calculations we can also numerically integrate the radial functions starting at $\xi=0$ with a slope of zero and an arbitrary value. It can be shown that this will give the correct form for the radial functions, but not the correct scaling. The radial functions must be scaled to match the Spherical Hankel Functions for large $k \xi$, because the magnitudes of both functions must asymptotically approach each other at large distances from the source. This process is not too difficult for us to contemplate, but it is a heck of a lot of work for the computer!

Fig. 6-5 shows the Oblate Spheroidal angular wave functions at $\mathbf{c}=5.0$ for a 30° waveguide. These functions are similar to the corresponding wave functions for a Spherical waveguide due to the relatively low frequency (\mathbf{c} value). This similarity between the functions supports our contention that at low frequencies nearly all shapes of waveguides with similar flare rates act just about the same, the flare rate being the only aspect of importance – i.e. it sets the location of the low-

6. See Press, *Numerical Recipes*, Chap. 11

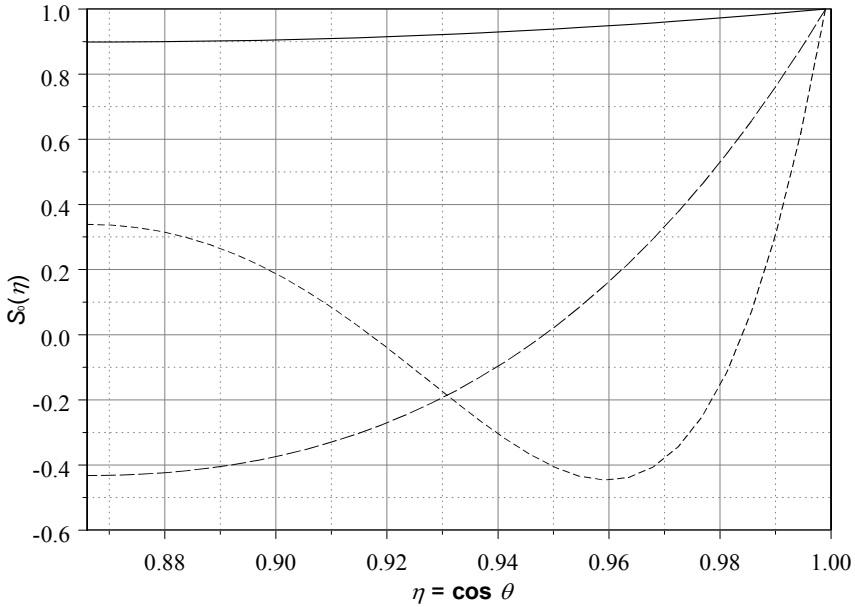


Figure 6-5 - Angular wave functions for 30° case, $c=5.0$

est frequency of significant transmission usually called cutoff. Of note in this figure is the fact that the lowest order mode, which is always independent of angle for a Spherical waveguide, is beginning to become curved with respect to θ in the OS waveguide. This means that even if we drive an OS waveguide with a flat piston, one which perfectly matches the aperture requirements for this waveguide, it will still generate higher order modes. This effect becomes greater as the frequency increases.

Fig. 6-6 shows the OS coordinate waveguide radial functions for both the real and imaginary parts for the 30° case at $c=5.0$. (The Spherical radial wave function - Spherical Hankel Function of the second kind - is also shown in these plots for reference.)

The imaginary parts of the radial wave functions can be very difficult to develop owing to the near singularity at the origin. The slope of these functions is known (from the Wronskian as shown below) but the values at the origin, which yields the proper asymptotic scaling, must be determined. Convergence of these functions requires a very high degree of accuracy in finding this value at the origin - about 15 significant digits for the $n=4$ mode at $c=5.0$. This makes it almost impossible to calculate these functions on a computer using standard iterative techniques for small values of c at the higher modal orders. The imaginary parts of the wave functions are usually required in order to calculate the modal radiation impedances. We will see a way around this situation shortly.

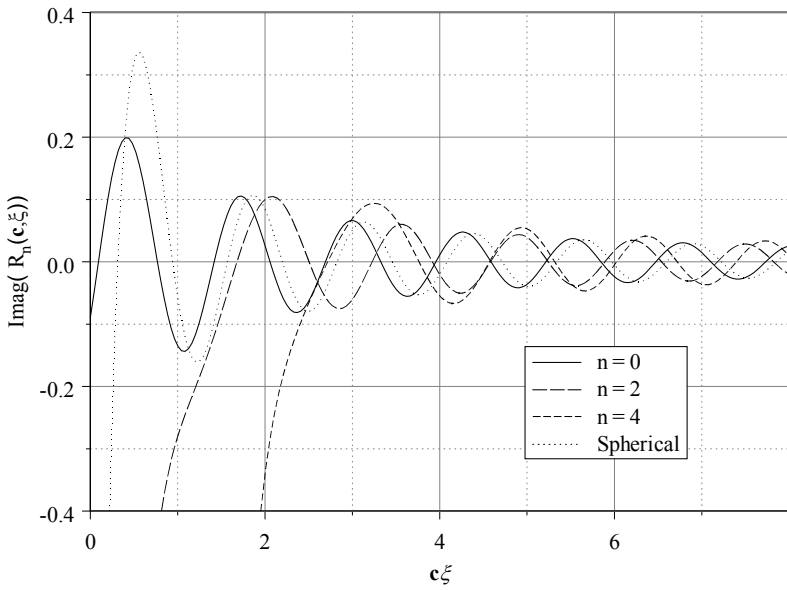
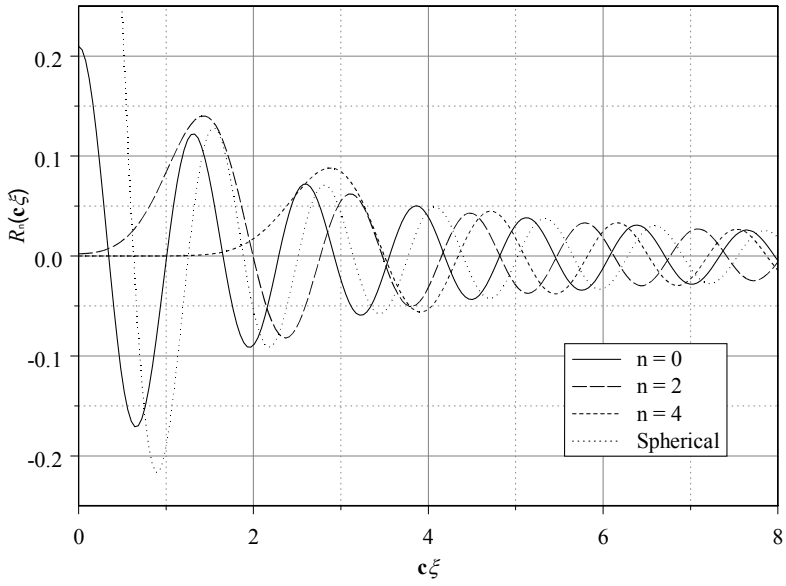


Figure 6-6 - The OS radial wavefunctions for a 30° waveguide at $c=5.0$

Fig.6-7 shows the angular wave functions for the same waveguide as in the previous figure but at a value of $c=10.0$. Here we see that lowest order wave function is becoming even more curved relative to the flat aperture at the throat. This means that there will be a significant amount of the $n=2$ mode present when this aperture is driven by a flat wavefront.

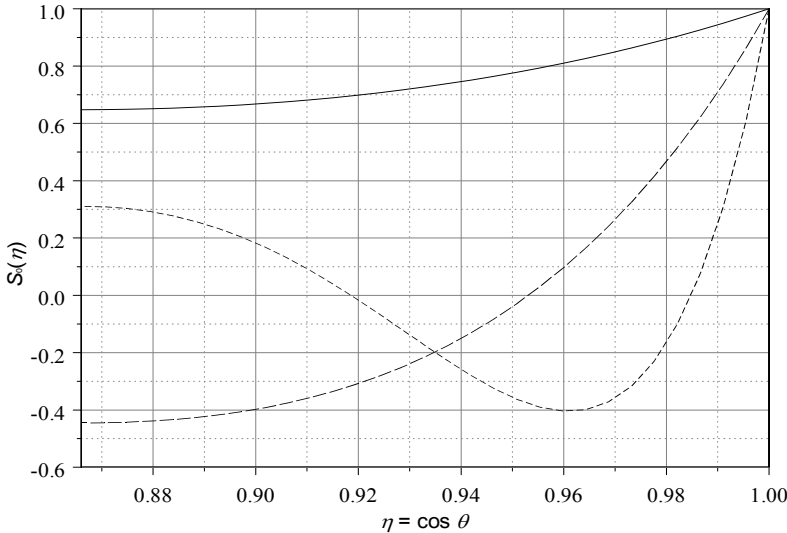


Figure 6-7 - Angular wave functions for 30° OS waveguide at $c = 10.0$

Fig.6-8 shows the radial wave functions for the 30° case at $c = 10.0$.

We can now compute the modal impedances for the radiation modes as follows.

- Calculate the radial wave functions finding the value required at the origin to yield the correct asymptotic values at high $c\xi$.
- Note that the Wronskian (a characteristic of all PDE's) for the OS Coordinates is

$$W(\mathbf{c}, \xi) = R^{(1)}(\mathbf{c}, \xi)R^{(2)'}(\mathbf{c}, \xi) + R^{(1)'}(\mathbf{c}, \xi)R^{(2)}(\mathbf{c}, \xi) = \frac{1}{\mathbf{c}(1 + \xi^2)}$$

which when evaluated at $\xi = 0$ yields

$$R^{(2)'}(\mathbf{c}, 0) = \frac{1}{\mathbf{c}R^{(1)'}(\mathbf{c}, 0)}$$

- Using this know slope for the radial wave function of the second kind at the origin, we can use ordinary integration to calculate the function to some large value of $k\xi$. Once again we compare the magnitude of this function to that of the Spherical Bessel Functions and iterate the

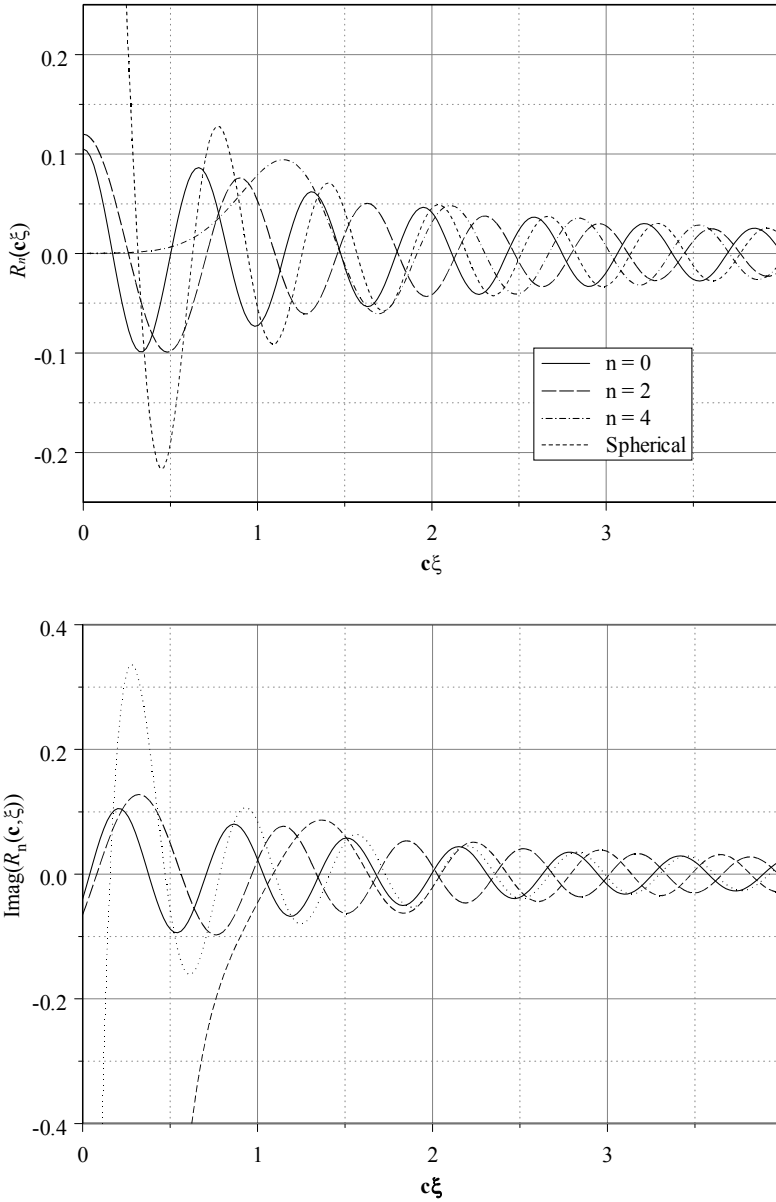


Figure 6-8 - The radial wave functions for a 30° waveguide at $c = 10.0$

starting value until the two functions match amplitudes at these higher radial values.

This is a tremendous amount of work, and the results are known⁷. We will not elaborate on the details of these calculations, but we will show the results. Fig.6-9 shows the modal impedances of the 30° waveguide for the first two modes. The third mode ($n = 4$) would not appear on this graph's scale. Thus only the first two modes are of significance for this waveguide over the bandwidth of interest. The second mode, $n = 2$, enters the picture at a value of $c \approx 7$, corresponding to a frequency of, (for a one-inch radius throat)

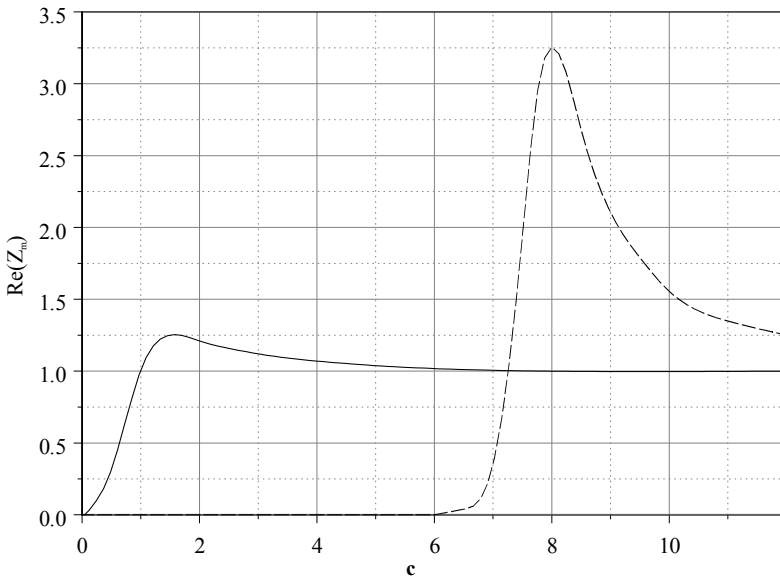


Figure 6-9 - impedance (real part) for 30° waveguide

$$f = \frac{c c}{\pi d} = \frac{c c \sin \theta_0}{2 \pi a} = \frac{7.0 \times 34300 \frac{\text{cm}}{\text{s}} \times \sin 30^\circ}{2 \times \pi \times 2.54 \text{cm}} \cong 7,000 \text{Hz}$$

Above this value, the second order mode will propagate with an equal or greater amount of influence than the “plane” wave mode, $n = 0$. In the vicinity of 7 kHz, this waveguide will becoming heavily dependent on the specific configuration of the components that control the wavefront at the throat (phase plug, etc.) Below about 5 kHz the wavefront geometry at the throat aperture is of little importance since only the lowest order mode – basically the average of the veloc-

7. See Geddes, “Acoustic Waveguide Theory Revisited”, *JAES*

ity of wavefront across the aperture – will propagate. At low frequencies, the details of the throat wavefront are irrelevant.

The $n = 0$ mode in the OS waveguide exhibits an impedance characteristic which is similar to that for a simple Spherical waveguide or conical horn. We must be careful in this comparison however, because even though the impedance and transfer characteristics for the OS waveguide are similar to those for a Spherical waveguide there are still significant differences.

Fig.6-10 shows the velocity distribution at the mouth for the 30° waveguide. (These are the velocity amplitudes normal to the spherical surface defined by the mouth.) These velocities are dependent on both the frequency and the angle θ . Note that the velocity gets greater at the center, and that this effect increases rapidly with frequency after about $c = 7.0$ where the second mode is becoming significant. This velocity distribution calculation at the mouth is one of the most important distinctions between waveguide theory and horn theory. Waveguide theory predicts a significant variation of the wavefront amplitudes across the mouth of the device even when driven by a uniform velocity distribution at the throat. Horn theory can only predict amplitudes which are independent of angle, which is clearly incorrect.

Consider now a 45° waveguide. Several things happen when we increase the waveguide coverage angle. First, the modes cut in at a lower value of c as shown in Fig.6-11. The second mode is now significant, above about 6 kHz and we can see that the third mode ($n = 4$) will be a factor in the passband of the device. The

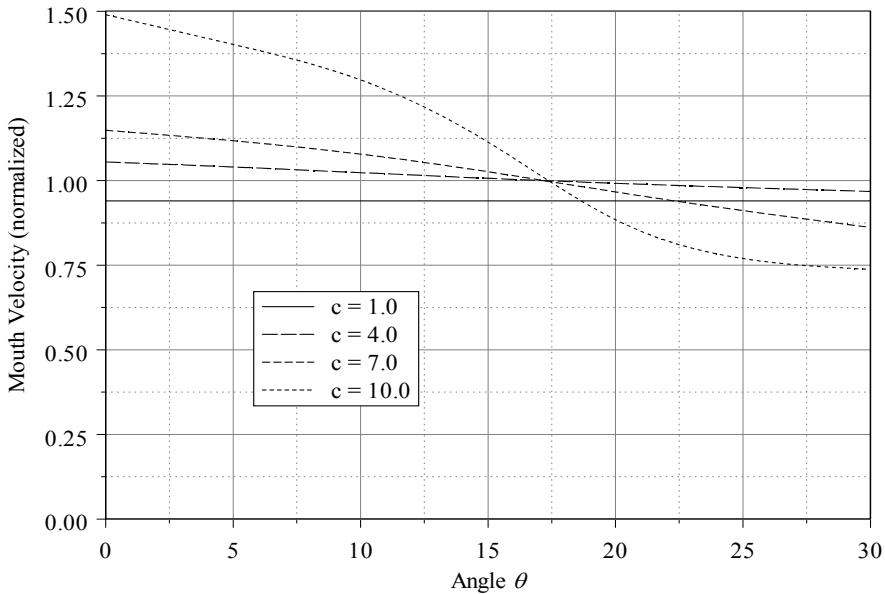


Figure 6-10 - Mouth radial velocity amplitude

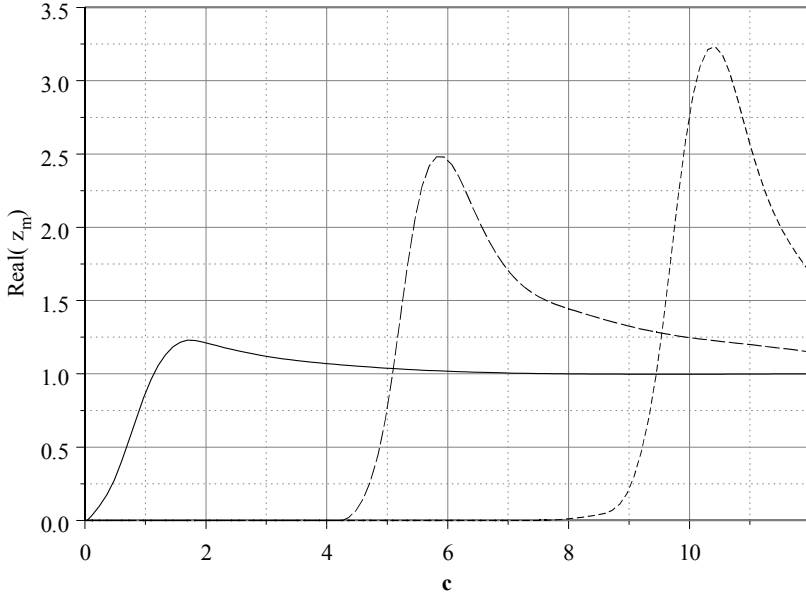


Figure 6-11 - The impedances for the 45° waveguide

next aspect of the angle increase is that the wave functions vary in θ to a greater extent with the larger angle. All of these effects add up to cause an even greater focusing of the wavefront velocities towards the center of the mouth. We have not yet shown whether this is good or bad, but it is important to note the effect.

If instead of driving the throat with a wavefront of constant amplitude we taper this amplitude as shown in Fig.6-12, then the net effect will be to create a distribution of the velocity at the mouth which has a far more uniform distribution than one fed with a flat throat velocity distribution⁸. This is an important result, for it means that better control of the sound radiation coverage of a waveguide can be achieved by manipulating the velocity distribution at the throat. Horn theory could never have predicted this result. Phasing plugs in compression drivers in common use today are principally designed to create a flat velocity distribution, because horn theory did not have the sophistication to consider anything else. The implications of this result to the phasing plug design is that, in essence, it must be part of the waveguide design and not part of the compression driver design. In the future phasing plugs will certainly be made to better adapt the device driving the waveguide to the requirements of the waveguide itself. The phasing plug is a variable in the design problem, not a fixed component.

At this point, it would be a good idea to review the key aspects of the waveguide theory developed in this chapter:

8. See Geddes, "Acoustic Waveguide Theory – Revisited", *JAES*.

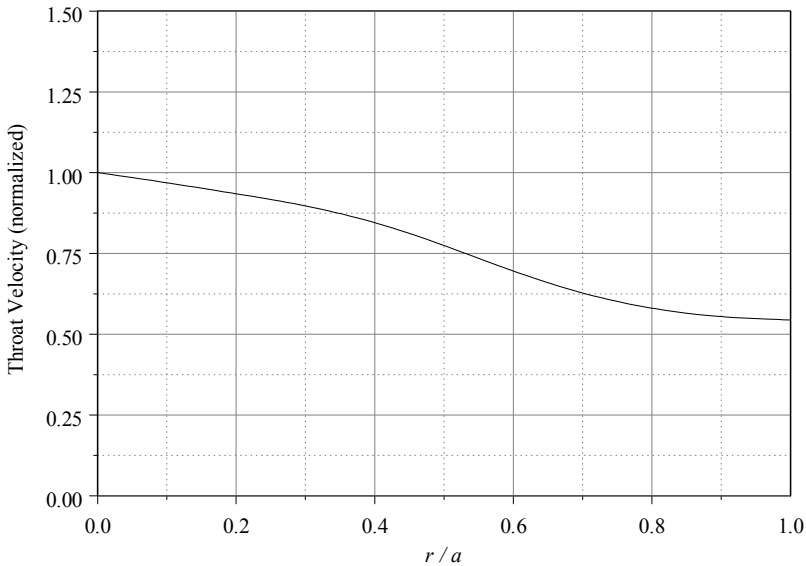


Figure 6-12 - Proposed throat velocity distribution for a flatter velocity distribution at the mouth

- All waveguides (as well as horns) have higher order modes. The fact that horn theory neither predicts nor is able to deal with this situation is a serious failing of the theory.
- The wavefront geometry (magnitude and phase distribution) at the throat of the waveguide is critical to its performance at higher frequencies.
- The loading aspects of nearly all waveguide/horn devices is, for all practical purposes, the same. The total encompassed solid angle of radiation is really the only factor influencing the loading.
- Horn theory is adequate only for the low frequency aspects of waveguides – well below the first mode cut-in and even then it gives no indication as to what the wavefront shape is at the mouth.

6.5 Approximate Numerical Calculations^{9,10}

We will now return to the discussion that we had in Sec.6.2 about an approximate method for the evaluation of a waveguide which does not conform to a separable coordinate system and yet retains those features from waveguide theory that are necessary for acceptable results.

The question is: can we find a way to do an approximate numerical calculation while still retaining the main features of waveguide theory? Clearly, any new technique must include the possibility for higher order modes, and it must be able to predict the actual wavefront distributions at the output (mouth) for any given distribution at the input (throat).

The way to do this is a modification of the obvious technique of breaking a waveguide down into a series of finite spherical sections. This is an old technique but we will add one new feature – we will track all of the modes, including the higher order ones, as they progress through the elements. We will only develop and outline this technique because time and space constraints will not allow us to show an example of its application. To do a thorough study of this technique and its implications would require far too much space. We will disclose the techniques and leave it to the reader to develop the applications.

Consider the geometry shown in Fig.6-13. The waveguide is broken into four sections where each section is a section of a cone in Spherical Coordinates. Calculation of the first order mode down this waveguide is trivial. It is done by simply multiplying together the T-matrices for each section to yield the composite matrix which represents the whole waveguide. The problem with this approach is that it ignores the presence and propagation of higher order modes within the waveguide, just as horn theory does.

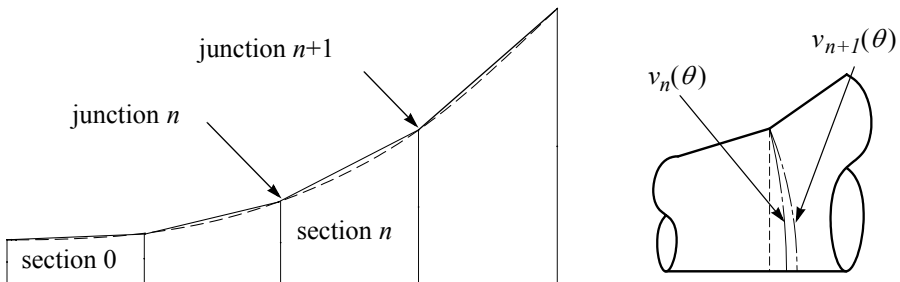


Figure 6-13 - A simple waveguide broken into sections and a detail of a single junction

9. See Mapes-Riordan, "Horn Modeling with Conical and Cylindrical Transmission Line Elements", *JAES*.

10. See Putland "Every One-Parameter acoustic Field Obeys Webster's Horn Equation", *JAES*.

It can be seen in the right hand side of this figure that at each junction between the sections, the wavefronts are not contiguous – the radius of these waves must change between the two sections at each junction. In order for this wavefront to propagate from one section into the next section we must match the wavefronts by creating higher order modes in the second section. These higher order modes are required for the wavefronts to match at the junction of the two sections. We will then have two (or more) modes which must be propagated through each of the following sections. This same situation will occur at each and every junction, thus continually increasing the higher order mode content of the wavefront.

The only way for this higher order mode creation to not occur would be for there to be a wavefront radius source point which did not move in space, as opposed to one that is changing in each section. It is now readily apparent that any waveguide which has a changing location of the origin for the wavefront radius will require the presence of higher order modes to account for this changing origin. In separable coordinates this changing radius location is exactly what the coordinate scale factors account for and exactly why the equations have become so much more complicated. This is another way of looking at the results that we elaborated on in the previous sections.

The entire concept of one-parameter (1P) waves is thus shattered by the realization that there can only ever be three waveguides, none of which are of interest to us, in which there can be true 1P behavior and then only if we feed them with non-existent sources. All other geometries and source configurations will have higher order modes no matter how we attempt to minimize them.

Furthermore, we cannot circumvent this problem by making more sections and thus a smaller change between sections, resulting in less higher order mode creation at each junction. The smaller values of the higher order mode components are multiplied many more times by the increased number of junctions, resulting in the exact same result that we have described above. There is simply no way around the conclusion that, in order to be accurate all waveguide calculations, we must include the presence of higher order modes or they are seriously flawed.

With this realization in mind we can be thankful that we have developed the machinery to deal with this complication, namely the T-matrix. By adding two more dimensions to the T-matrices – for each higher order mode that we want to calculate – we can accommodate this new complication. We will have larger matrices to deal with (4x4 for two modes, 6x6 for three modes and so on), but we'll let the computer deal with that problem.

The T-matrix for the two mode spherical element is easily derived from the Spherical Wave Equations by using techniques identical to those we used in Sec. 5.2 on page 95, only now we are using two modes in Spherical Coordinates.

Without belaboring the details in the derivation of the T-matrix for this problem, the results are

$$\begin{bmatrix} p_n^0 \\ v_n^0 \\ p_n^2 \\ v_n^2 \end{bmatrix} = \begin{bmatrix} [T_n^0] & \tilde{0} \\ \tilde{0} & [T_n^2] \end{bmatrix} \begin{bmatrix} p_{n+1}^0 \\ v_{n+1}^0 \\ p_{n+1}^2 \\ v_{n+1}^2 \end{bmatrix} \tag{6.5.13}$$

p_n^m = the modal pressure m at junction n

v_n^m = the modal velocity m at junction n

m = mode number

n = section-junction number, section n has junctions n and $n+1$

and where

$$T_n^m = \begin{bmatrix} H_{0,0} & H_{0,1} \\ H_{1,0} & H_{1,1} \end{bmatrix} \cdot k^2 r_{n+1}^2 \tag{6.5.14}$$

$$H_{0,0} = \left(h_{v_m}^{(1)}(kr_{n+1}) \quad h_{v_m}^{(2)}(kr_n) - h_{v_m}^{(1)}(kr_n) \quad h_{v_m}^{(2)}(kr_{n+1}) \right)$$

$$H_{0,1} = \left(h_{v_m}^{(1)}(kr_{n+1}) \quad h_{v_m}^{(2)}(kr_n) - h_{v_m}^{(1)}(kr_n) \quad h_{v_m}^{(2)}(kr_{n+1}) \right) \cdot i\rho c k$$

$$H_{1,0} = \left(h_{v_m}^{(1)}(kr_{n+1}) \quad h_{v_m}^{(2)}(kr_n) - h_{v_m}^{(1)}(kr_n) \quad h_{v_m}^{(2)}(kr_{n+1}) \right) \cdot \frac{-i}{k\rho c}$$

$$H_{1,1} = \left(h_{v_m}^{(1)}(kr_n) \quad h_{v_m}^{(2)}(kr_{n+1}) - h_{v_m}^{(1)}(kr_{n+1}) \quad h_{v_m}^{(2)}(kr_n) \right)$$

$h_{v_m}^{(1)}(kr)$ = the Spherical Hankel Function of the first kind of order v_m

$h_{v_m}^{(2)}(kr)$ = the Spherical Hankel Function of the second kind of order v_m

v_m = the Eigenvalue for mode m with the specific angle of section n

h' = the derivative of the function with respect to its argument

r_n = the radius to the entry aperture for section n

r_{n+1} = the radius to the exit aperture for section n

This is a complex result – one best left to a computer to sort out. In the case of the lowest order mode it can be simplified significantly and turns out to be

$$T_0 = \frac{r_2}{r_1} \begin{bmatrix} \cos kl - \frac{\sin kl}{kr_2} & -i\rho c \sin kl \\ \frac{-i}{kr_1 \rho c} \left(\left(\frac{r_1}{r_2} - 1 \right) \cos kl + \left(kr_1 + \frac{1}{kr_2} \right) \sin kl \right) & \cos kl + \frac{\sin kl}{kr_1} \end{bmatrix} \tag{6.5.15}$$

$$l = r_2 - r_1$$

From the numerical standpoint it is best to leave the matrix in the form shown in Eq.(6.5.14) above. The wave functions can be made as a single call to a subrou-

tine with the correct arguments. In fact only two calls need to be made for each mode since the subroutines return four values, the values of the functions of the first and second types along with their derivatives, all of which are required.

The procedure for the application of this technique is to start at the throat, calculating the modal contributions of the wavefront found at that location in terms of the angular modes appropriate for that section. These modes are then propagated to the next junction using the matrices shown above, at which point the wavefront (the sum of the modal wavefronts) is again expanded in terms of the angular modes appropriate for the next section. In order to do these calculations we will need to know the Eigenvalues as a function of the sections angle.

These Eigenvalues can be calculated using the same shooting technique from the previous section. Then a simple equation is fit to the data. The exact values (circles) and the fitted equation are both shown in Fig. 6-14. The equation for this fit is

$$\lambda(\theta) = \frac{21}{(\sin \theta)^{1.87}} - \frac{12}{\sin \theta} \tag{6.5.16}$$

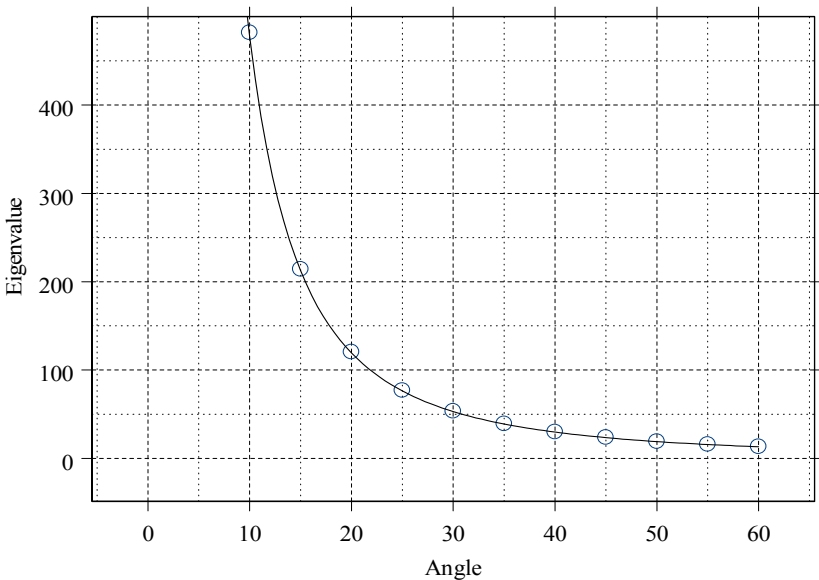


Figure 6-14 - Eigenvalues for a Spherical waveguide versus angle

With the eigenvalues known it is an easy matter to generate the “allowed” angular functions $S_n^m(\cos \theta)$ in each section. In order to find the contribution of each mode at each junction, we must pick a surface on which we can expand both sets of functions – those in the incoming section into those in the outgoing section. The simplest surface on which to do this is a planar one through the junction.

Expanding the velocity function $v_{n+1}(\theta)$, as shown in Fig.6-13, at junction $n+1$

$$v_{n+1}(\theta) = \sum_{m=0}^{\#modes} v_{n+1}^m S_n^{V_m}(\cos \theta) \tag{6.5.17}$$

where v_{n+1}^m is obtained from Eq.(6.5.13). We can calculate the complex velocity distribution of a spherical wave onto the flat disk at junction $n+1$. We need to slightly modify the values that we found in Sec.4.2 on page 75 to account for the presence of the higher order modes as

$$v_{n+1}(\sigma) = v_{n+1}(\theta) \frac{l_n^2}{l_n^2 + \sigma^2} e^{ik(\sqrt{\sigma^2 + l_n^2} - l_n)} \tag{6.5.18}$$

$$\theta = \frac{\sigma}{\sqrt{l^2 + \sigma^2}}$$

$v_{n+1}(\sigma)$ = the normal velocity function on the planar disk at junction $n+1$

l_n = the length from the virtual apex of element n to junction $n+1$

This equation represents the complex normal velocity distribution across the waveguide at junction $n+1$.

We now need to expand this velocity function into the angular modes of section $n+1$, $S_{n+1}^{V_m}(\cos(\theta))$. The modal velocity contributions at the input to section $n+1$, v_{n+1}^m , will then be

$$v_{n+1}^m = \int_0^{\eta_{n+1}} v_{n+1}(\eta) S_{n+1}^{V_m}(\eta) d\eta \tag{6.5.19}$$

$\eta_n = \cos(\theta_n)$ the angle of the n th section

$\theta_n =$ angle of section $n+1$

The calculation procedure then becomes:

- calculate the modal contributions at the throat v_0^m
- propagate these modes to junction 1 using Eq.(6.5.13)
- using Eq.(6.5.17), find the angular velocity $v_1(\theta)$
- find the normal velocity on the matching disk $v_1(\sigma)$ from Eq.(6.5.18)
- expand $v_1(\sigma)$ in terms of the new angular functions in section 1 from Eq.(6.5.19)
- loop through all sections to end junction – the mouth

It is interesting to note that the above problem can also be worked in reverse. That is, we can start with a desired mouth wavefront and work back to the throat in order to determine what the wavefront should be at that surface in order to achieve the wavefront that we want at the mouth. It is simply a matter of taking

the inverse of the matrix from the throat to the mouth. The problem is that we have not said anything about what the mouth wavefront should be in a particular situation. We have looked at the issue of analyzing a given device, but not, finding the optimum device. We will find in later sections that the entire problem can be worked in reverse, namely, we can specify a desired polar response field, calculate the required mouth velocity distribution to achieve that field, and finally work backward to find a throat distribution needed to achieve the desired polar response. With any luck we could design a phasing/amplitude plug for the driver to give us the throat velocity that we want.

6.6 Treatment of Mouth Diffraction

Up to this point we have not talked about the diffraction of the waveguide wavefront at the mouth of the device. There will always be a termination of the waveguide since no waveguide can be of infinite length. We need to understand how the mouth diffraction will affect the polar response. First, however, we should understand what our target polar response needs to be in order to know what mouth velocity we will want. The obvious question “what polar response do we want?” will not be resolved here; there probably is not a single answer. However, we will attempt to shed some light on this topic in the chapter on room acoustics. For now, let’s just simply assume that what we want is a controllable radiation pattern of some nominal angle, say 30° , since this is the angle that we have been using in our examples thus far.

It may not be obvious that we can work the polar radiation problem backwards. Namely, that given a desired polar response we can use our modal radiation tools in reverse to calculate the velocity distribution required on a flat or more appropriate to a waveguide, a spherical surface. The process is to expand the desired field into its fundamental radiation modes and then to calculate (in reverse) what the amplitude and phase of these modes would have to be at the source to yield the desired radiation pattern.

Knowing that this reverse problem is a transform, let’s consider some characteristics of the problem that we should expect. The most important is the k-space equivalent of the well known energy-time trade-off in sound measurements. The more confined, narrower, the polar response is the broader we should expect the source velocity to have to be to achieve this result. This implies that since our source is finite in size, we could easily ask for a polar pattern which cannot be achieved by the given source. We should expect a gradual rate of change of the polar response with angle if we want to achieve a smooth velocity distribution across the mouth of the waveguide and hence across the throat. This last aspect is analogous to a filter, where a sharper cutoff requires more coefficients in the filter – in essence, a “high order” filter. High order velocity distributions mean a lot of radiation modes, but we already know that we will have three or at most four modes within the waveguide to work with and then only above the frequency of

the particular mode's cut-in/off. So clearly the best that we could hope to achieve is a fairly low order polar response, i.e. a gradual change in response with angle.

As an example of the characteristics that we have been talking about, consider the unrealistic polar response where the pressure is

$$p(\theta) = \begin{cases} 1 & \theta < 30^\circ \\ 0 & \text{otherwise} \end{cases} \tag{6.6.20}$$

We can calculate the required radiation modes as follows. From Chap.3 we know

$$p(r, \theta) = -i\rho c \sum_n \left(n + \frac{1}{2}\right) \frac{V_n}{h'_n(ka)} P_n(\cos \theta) h_n(kr) \tag{6.6.21}$$

$V_n =$ the (unknown) modal velocity components at the spherical surface

$a =$ the spherical radius, basically the length of the waveguide

$r =$ the distance to the measurement surface

from which, using orthogonality for the Legendre Polynomials and a known function $p(r, \theta)$, we will find

$$V_n = \frac{h'_n(ka)}{-i\rho c h_n(kr)} \cdot \Pi_n \tag{6.6.22}$$

where

$$\Pi_n = \int_{-\pi}^{\pi} p(r, \theta) P_n(\cos \theta) \sin \theta d\theta$$

If we are interested only in a far field directivity function, then the denominator terms in Eq.(6.6.21) constitute a complex constant that is the same for every mode except for a factor $-i^n$, which comes from the large argument approximation to the Hankel Functions. Any term which is independent of n simply scales the coefficients. Since we will be looking at normalized directivity functions, these constants will therefore be unimportant. (If we want to look at the frequency response at some point then, of course, we will need to retain these terms.)

Finally, we can simplify Eq.(6.6.22) to get

$$V_n = -i^n h'_n(ka) \Pi_n \tag{6.6.23}$$

Once we have these velocity modes the velocity distribution in the mouth will be

$$v(\theta) = \sum_n V_n P_n(\cos \theta) \tag{6.6.24}$$

Fig.6-15 shows the calculated mouth velocity profile required to achieve the desired polar pattern.

These results need some explanation. First, they are not stable with different values of n , the number of modes in the calculations. The velocity profiles become unstable – wide oscillations, as one adds more and more terms in the

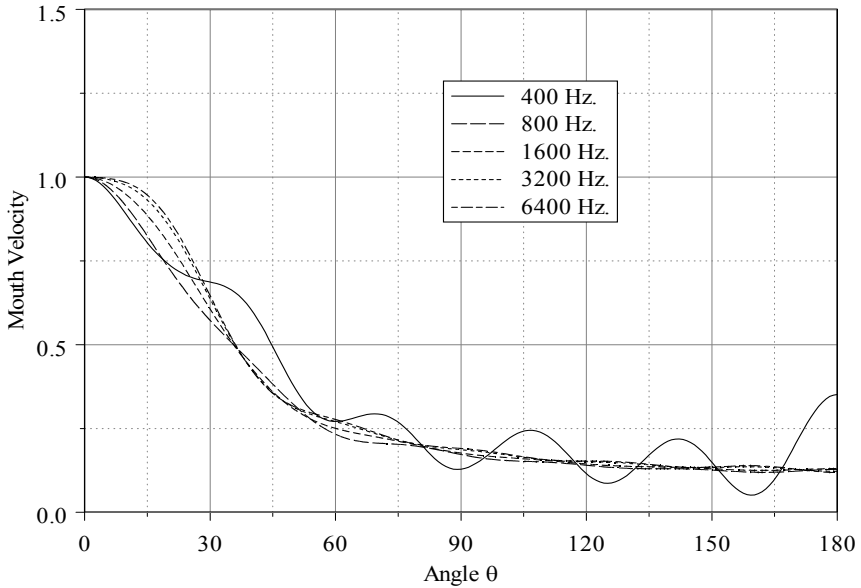


Figure 6-15 - Velocity magnitude for 30° abrupt polar response

expansion. This is understandable since the higher order terms are attempting to fit the sharp discontinuity in the polar response. Then another problem occurs for the specific case shown here in that these velocity patterns are frequency dependent. If we are going to “sculpt” a mouth velocity we must pick one of these curves. We could attempt to match different profiles at different frequencies, but we would quickly find this unworkable. It is reasonable to expect to be able to create an approximately frequency independent mouth wavefront by the proper design of a waveguide and its phasing plug (or perhaps a slight frequency dependence if it follows the natural modal changes that we saw in section 6.4), but it is unreasonable to assume that we could have a specific frequency dependence in a prescribed manner, such as in the figure above.

Another issue is the fact that the velocity profile goes all the way around the sphere, which is unrealizable in practice. Even if it were realizable it is still undesirable. The limits of our velocity control, namely, the mouth size for a 30° device of a given length, will force us to terminate the velocity profile at this same angle. The method for terminating the velocity profile is critical to achieving our desired results.

We can pick a profile from Fig. 6-15, terminate it at 30° , and recalculate a new set of modified V_n 's. We can then use this new set of coefficients to calculate an expected polar pattern. A polar map of the response for an abruptly terminated mouth velocity is shown in Fig. 6-16. The waveguide here is a $\pm 30^\circ$ device with a length of 1.0m. The mouth would be about 1.0m across, in an enclosure (a sphere) 2.0m in diameter, which is a fairly large device.

Once again we need to elaborate on some characteristics of this plot. There are 50 modes used in the summation for this pressure response. Remember that these are the modes for the sphere which is much larger than the waveguide or its mouth. This means that many more modes are required for convergence of the solution. By changing the number of modes used these plots and noting where the plots change (i.e. at what frequency) we can estimate the number of modes required for accurate results at any frequency. The results shown in Fig.6-16 are estimated to be good to about 4.5kHz. We can see a distinct change in the response at about this frequency. The peculiar response at about 2.5kHz. is real.

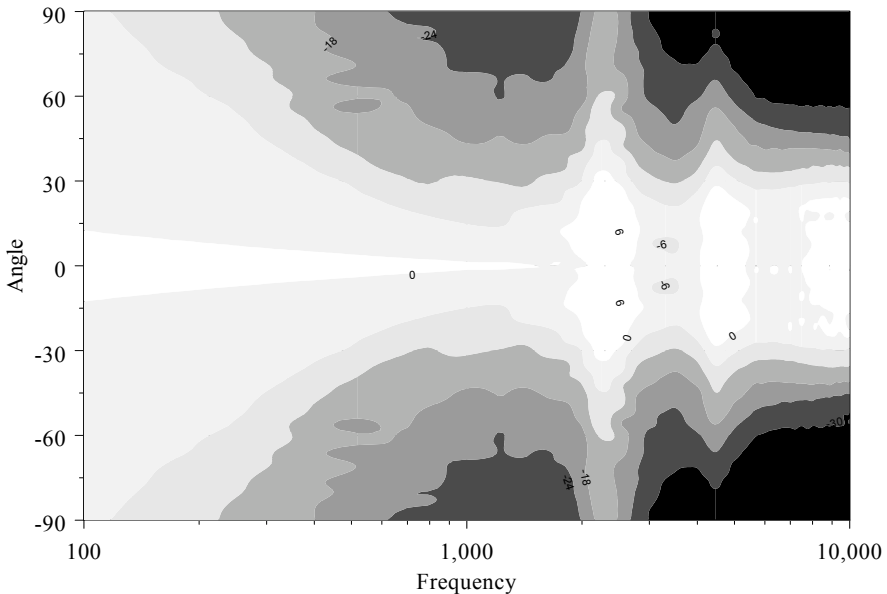


Figure 6-16 - The polar response map for a waveguide with an abruptly terminated mouth

Finally, these polar maps are all normalized to a level of 0dB on axis. This brings up an important point that perhaps we should wait to make until we talk about room acoustics, but we will discuss it here. It is always possible to electronically equalize the response of any loudspeaker system along any horizontal line in one of these polar maps. We almost always do this along the axial line. It is important to realize, however, that it is impossible to electronically correct the entire polar map. Its simply cannot be done. The implication here is that electronics can only go so far in the correction of a loudspeaker's problems. The rest is up to the designer.

Remembering the basics of the transform relationships for the velocity-polar response, perhaps it would be more logical to design to a polar pattern that does not change as abruptly with angle as the "step response" polar pattern used

above. We will find it convenient to deal with polar response functions of the following form

$$p(\theta) = e^{-a\theta^2} \tag{6.6.25}$$

a = the rate at which the polar response falls off with angle

A value of $\alpha = 1.25$ gives a -3dB point at about 30° as shown in Fig. 6-17. The polar response is independent of frequency so a polar map (level versus angle and frequency) is not required.

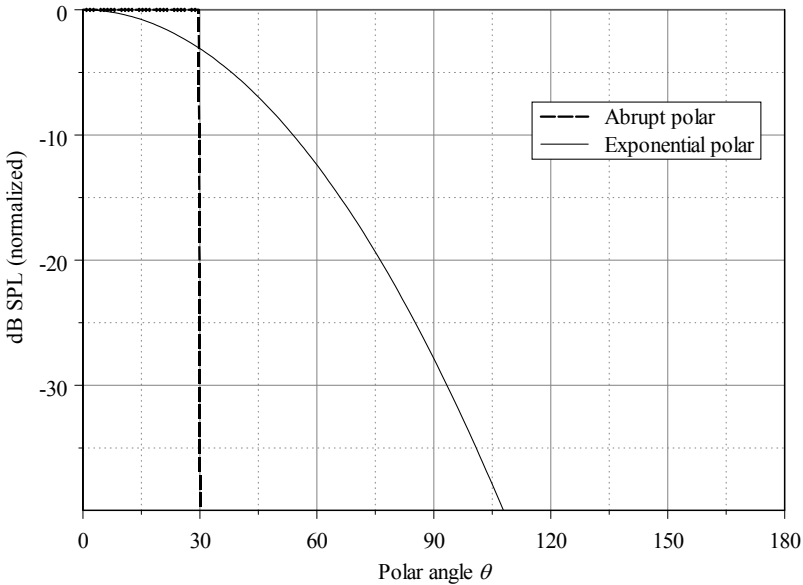


Figure 6-17 - Intended polar patterns – abrupt and exponential

The calculated velocity distribution for this exponential polar response is shown in Fig. 6-18. This curve is created using 20 modes in the summation. The instability of the inverse calculation can clearly be seen in the 400 Hz curve. At some number of modes all of the curves become this complex. Here we can see that if the curve is not oscillatory then it will be identical to all the over curves. This is attractive since there is now no ambiguity about which curve to choose as our target distribution. The fact that the velocity wraps completely around the source is still a problem. Otherwise this velocity distribution appears to be realizable at all a frequencies.

It is interesting to note that the velocity distribution in Fig. 6-18 goes well beyond the 30° point on the sphere, which is in stark contrast to the established principle of “line of sight” directivity of a spherical source. The wide angular velocities required to yield a 30° coverage pattern suggests the possibility of using

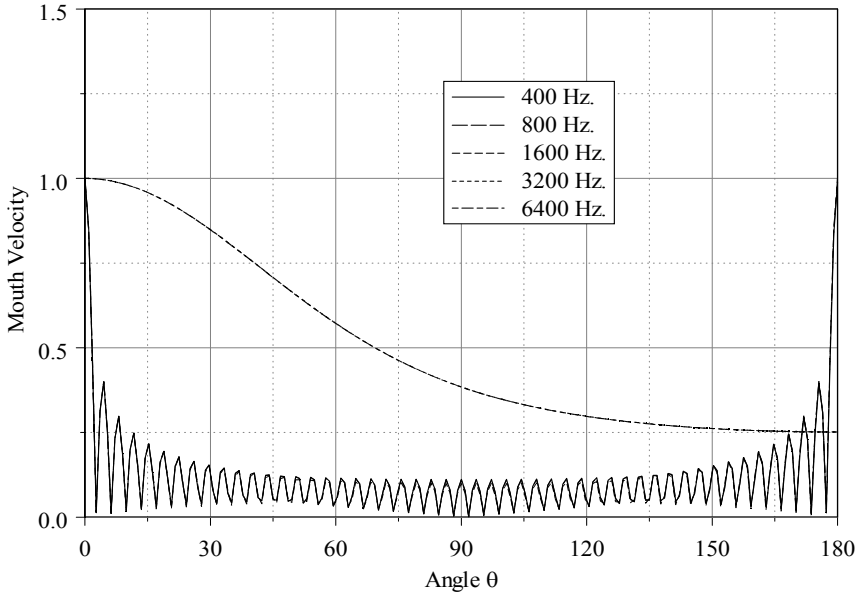


Figure 6-18 - The source velocity magnitude for a smooth polar pattern

a much wider waveguide angle to yield an improved narrower angle response, an option that we will be developing later.

If we terminate the waveguide at the baffle in an abrupt manner we would find that we would not get a polar response any better than what we saw in Fig.6-16. This implies that abruptly terminating the velocity profile in the spherical surface of the source is not something that we would ever want to do. There may be a better way.

If we flare the waveguide into the baffle by applying a large radius (“large” being something that we will define in a moment) from the body of the waveguide into the baffle, instead of an abrupt termination, then we will find that we can get a polar response much more to our liking. Unfortunately, flaring a waveguide into the baffle is not a precise thing to describe mathematically. For our purposes here, we will assume that the flare has the function of tapering the velocity found at the mouth in a gradual fashion, as shown in Fig.6-19. This plot has an abscissa that is an angle, but it can also be thought of as the radius out from the center of the mouth to the outside edge in the hypothetical spherical surface of the enclosure, i.e. the waveguide’s mouth.

The predicted polar response map for this new velocity distribution is shown in Fig.6-20. This response is nearly ideal with nearly constant coverage at 30° (-6dB points) from about 400Hz and up.

There are several things to note from the results to this point. First, it is possible, and reasonable, to do a waveguide design backwards by specifying the desired

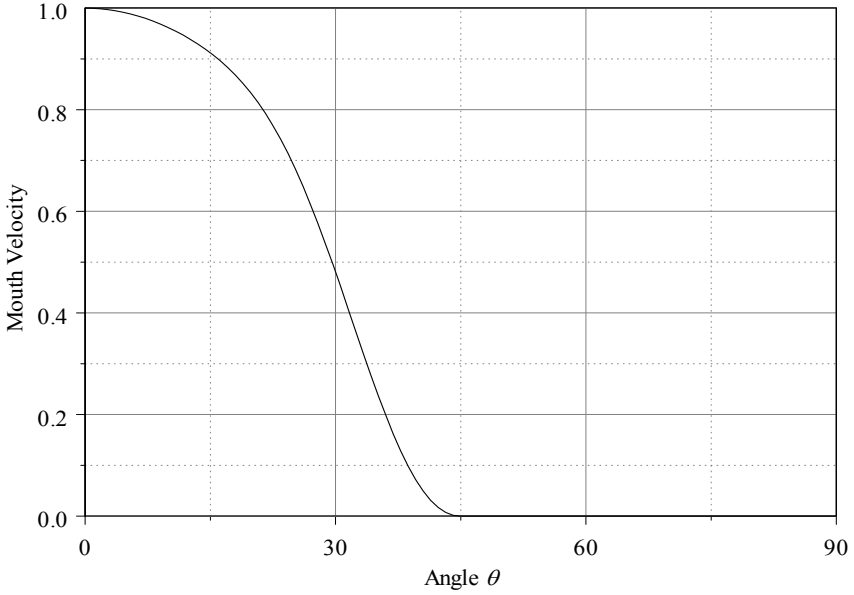


Figure 6-19 - Velocity distribution for flared waveguide

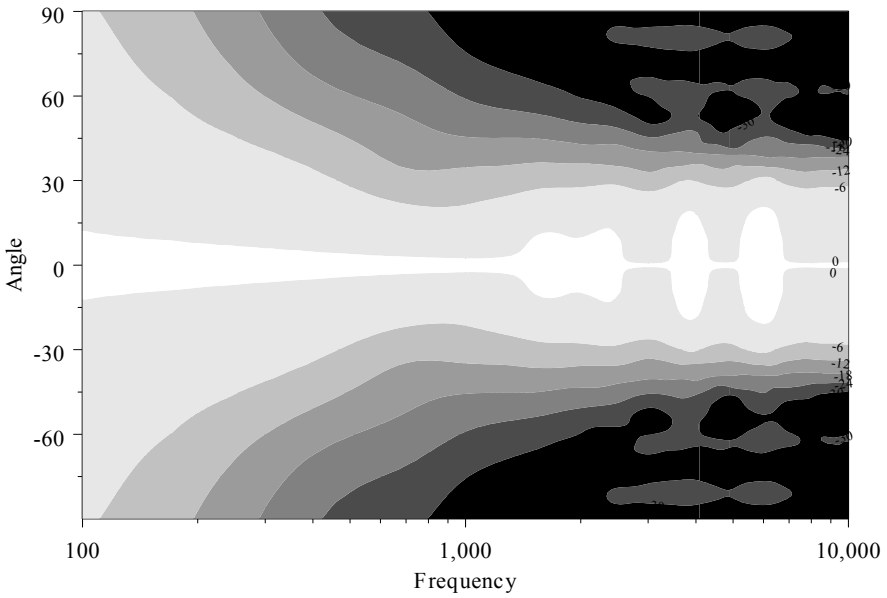


Figure 6-20 - Polar map for a flared waveguide

polar response pattern, calculating the required mouth velocity; back propagating this contour through the waveguide to find the required throat velocity, and finally designing a phase plug that achieves this required throat velocity. Second, for constant directivity we do not want a wavefront with a velocity contour which is independent of angle (radius), i.e. flat, and finally, that waveguides should always be flared into the baffle and never left with an abrupt termination since this secondary diffraction is uncontrolled.

Returning now to the discussion that we started earlier regarding a larger waveguide angle possibly achieving a better polar response, consider the velocity profile shown in Fig.6-21. This corresponds to a larger angular coverage ($> 30^\circ$)

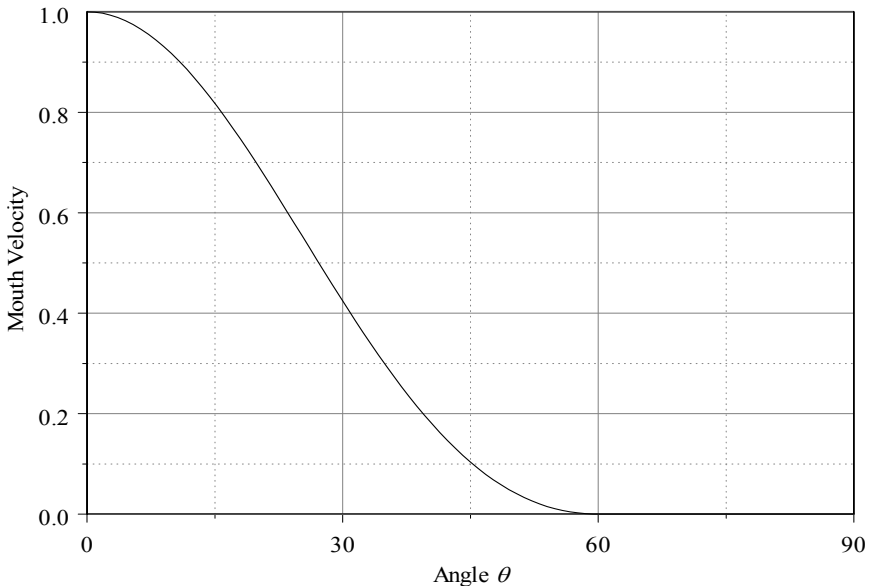


Figure 6-21 - Optimized velocity profile

with a more gradual falloff of the velocity with angle (radius). The polar map is shown in Fig.6-22. This polar response is virtually the ideal: -6dB at 30° from 400Hz-10kHz. While it is not obvious how one would obtain the velocity profile shown in the figure it certainly seems possible. For instance one might make a waveguide which had absorptive boundaries rather than reflective ones. This would reduce the velocity profile at the edges relative to the center in a manner similar to that desired. We could, in fact, analyze this situation by developing wave functions in the waveguide which had an impedance at the boundary instead of a zero velocity condition. (Yet another interesting exercise for the reader.)

While complex, the task described above is certainly not impossible. The point here is that while the response shown in Fig.6-22 may seem unreachable *it is* theoretically possible. Experience has shown that what is possible can be achieved.

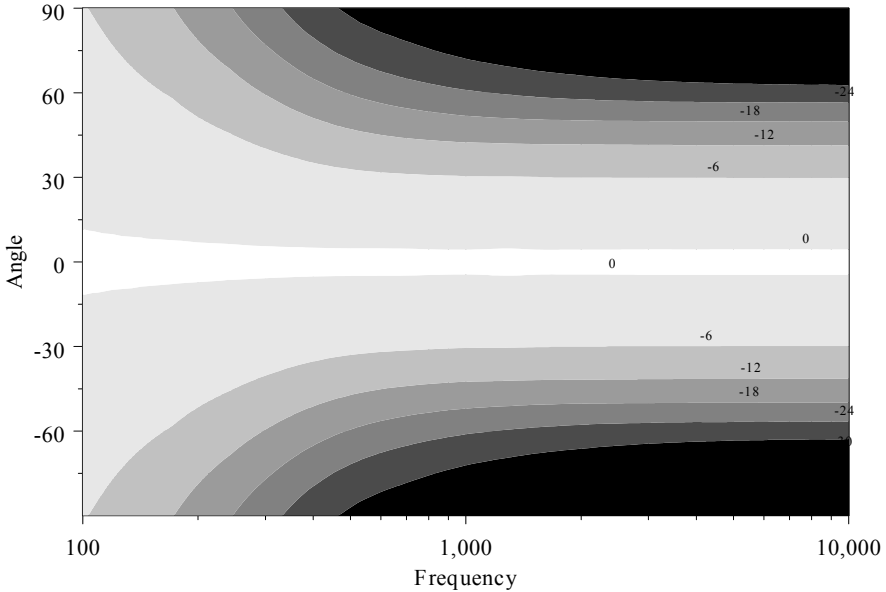


Figure 6-22 - A polar pattern with smooth angular variation

Compare the figures in this section with those in Chap.4 for various uncontrolled sources. It is apparent that without some form of waveguide, one is forced to deal with uncontrollable and undesirable situations in regard to the polar response. We have clearly shown that this situation does not have to be accepted as a constraint of the design problem. Waveguides offer a means to control the directivity yielding almost any polar response that is desired.

Waveguides do have limitations. Most notably, it is difficult to obtain wide directivity with good control. We have also not discussed how to obtain non-axis-symmetric polar patterns. The former problem will be discussed in later chapters when we talk about arrays and the latter problem is really not so difficult. A study of the separable coordinate systems highlights the Ellipsoidal (ES) Coordinates as having an elliptical mouth and these devices would yield a non-axis-symmetric polar pattern. Using them is really not much different than using the OS, except that the boundaries are defined by an elliptic equation which is not so widely known. Not much would likely be gleaned from doing an analysis of these devices (so we will leave that task to the interested reader), although, as we pointed out in Chap. 2, the wavefunctions in these coordinates are not known. One final point here is that the ES Coordinates require an elliptical throat, which of course is easy to achieve in the phasing plug design. This is one more reason why the phasing plug design must be part of the waveguide and not the driver.

6.7 Diffraction Horns

It would not be fair to leave this chapter without mentioning the horn design which has dominated the marketplace for so many years. Diffraction horns are devices which obtain their control by diffracting the wavefront and then constraining it to some confined angle via a sort of conical contour.

A typical layout of a diffraction horn is shown in Fig.6-23. This drawing shows a top view and a side view in cross section. The side view is basically the top view swung through an arc of the desired vertical polar pattern. Many variations on this construction are possible, but this drawing shows the device in its simplest embodiment.

From Chap.4 we know that when the radiating surface is small compared to the wavelength, then the polar response is wide (recall the transform of a Rect

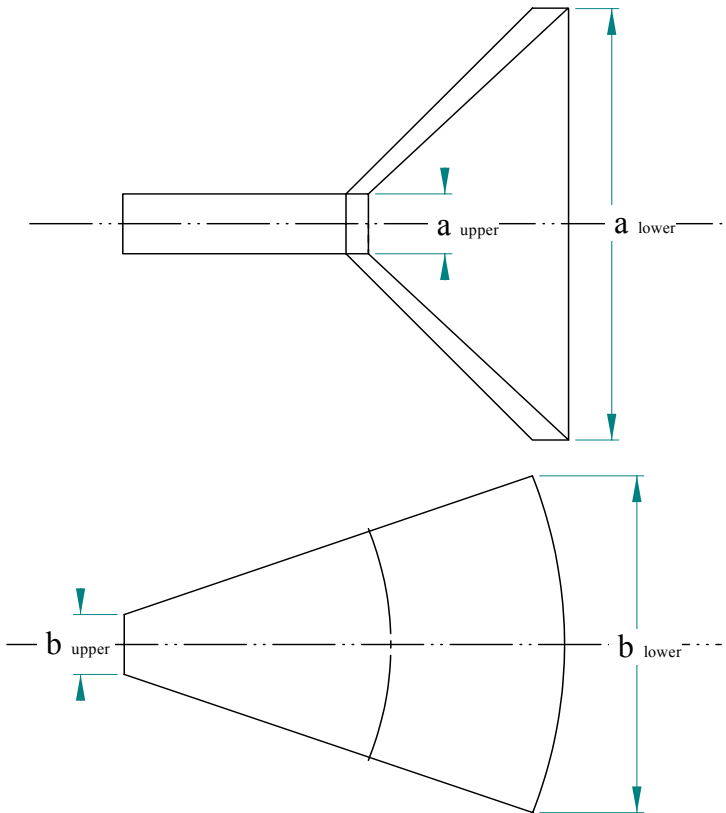


Figure 6-23 - Typical layout of a diffraction horn

function, which widens as the function narrows.). A diffraction device usually works on the horizontal and vertical axis as separate designs, thereby allowing for different patterns in the two directions. The throat is initially an exponential horn owing to the fact that most compression drivers have exponential sections in their phasing plugs. It initially expands in only one dimension – usually the dimension with the narrower pattern, the other dimension remains constant at a value chosen so that it is no wider than a half wavelength at the highest frequency of control.

At some point this initial horn is terminated. The exact location, distance from the diaphragm, is not critical and is usually chosen as a compromise for convenient forming of the horn and to set the desired distance that we will discuss below. The diffraction slot is usually an abrupt slope discontinuity although it can also be rounded – which tends to smooth out response ripples caused by the diffraction and reflection at this junction. After the diffraction, slot the device flares in both dimensions and is usually straight sided at this point (although some curvature is often found to be useful.) The angles of the sides are set to the desired coverage pattern, where the line-of-sight rule-of-thumb is the design concept. The diffraction slot can be either curved (as shown) or flat depending on the design. This aspect makes little difference except that the reflected wave, which we will talk about later, is not as coherent in the flat slot as it would be in the curved one. This tends to spread the reflection ripples slightly.

The value of $ka_{upper} = \pi$ basically sets the upper limit of horizontal control while ka_{lower} will set the lower limit of this control. The same is true for the horizontal dimension where kb_{upper} controls the highest frequency and kb_{lower} the lower frequency. It should be apparent that the design does not allow for independent control over all of these variables. It is this latter factor and the need to compromise that leads to the wide variations seen for this design.

The throat of a compression driver is usually round (although a rectangular phasing plug would allow for a greater flexibility in the design compromise) and so the initial section usually transitions from round to square in some manner. The final horn contours are usually flared to a certain extent because this has been found to be advantageous. Flaring into the baffle is also seen and not seen depending on the designer.

The problem with a diffraction horn is the large amount of energy reflected from the diffraction slot. There is (must be) a large impedance mismatch at this slot in order for the device to work, i.e. in order for there to be sufficient diffraction to work with. This impedance mismatch will reflect a great deal of the incident wavefront back down the device. A standing wave results, which is evident in both the electrical impedance of the driver as well as the frequency response of the system.

A second problem with the diffraction device is the ambiguity of its acoustic center. That is because there are actually two. One is at the throat of the device and the other at the diffraction slot. The plane in which the sound wave has been diffracted will have the diffraction slot as its acoustic center and the other plane

will have the acoustic center at the throat. At angles not in one of these planes the acoustic center is ambiguous. This causes problems with arraying these devices, because, as we shall see, the location of the acoustic center is the crucial point in array performance.

While diffraction horns have served the market well, they are now basically obsolete. The wavefronts in these devices are complex and can only be analyzed with complex numerical codes like FEA. At their best, their performance can be as good as a well designed waveguide and at their worst, they can be a disaster. This, of course, is only our opinion, but we hope that the reader will recognize that the results shown in this chapter support such an opinion.

6.8 Summary

A long and complex chapter the subject matter presented here is none the less of crucial importance to the design of loudspeaker systems. We showed that we must seriously question the use of the Horn Equation for waveguide design as it is inapplicable. However, the fact remains that some horns designed from this equation have worked well. From our results, we can see that the diffraction that occurs in an exponential horn (for example) could yield exactly the right mouth wavefront, but if it did it would be purely a coincidence! There is no way that one could design such a successes from horn theory.

We have attempted to point out that controlling the polar response of the system is possible, albeit not easy. We will see in later chapters that directivity becomes a major component in the design of loudspeaker systems once one includes the room effects in this design. This is true for both the large and small venues, but for different reasons. In either case, it just does not seem reasonable to accept as fact that loudspeaker systems have to have directivity properties which are uncontrolled, or omni-directional. (Omni-directional being, in our opinion, not really controlled, but simply the acceptance of the notion that nothing else is possible.)

It is true that the recent trend towards smaller and smaller loudspeakers does not allow for directivity control to any appreciable degree. Directivity control below the frequency where the dimensions of the enclosure become comparable to the wavelength of the sound cannot be accomplished without substantial amounts of signal processing and multiple drivers – an expensive proposition and not one that we are likely to see with wide availability in the near future. While the idea that enclosures need to be large for good low frequency response is certainly true, we can see that there is now another reason for larger enclosures – the ability to control the directivity/power response of the loudspeaker system. The authors hope that good sound quality demands will prevail and that we will see a return to the “substantial” sized loudspeakers of the past in the modern applications of home theatre and other applications where sound quality is a primary consideration.